Mon. Not. R. Astron. Soc. **346,** L16–L20 (2003)

# A search for starlight reflected from HD 75289b

Christopher Leigh,[1]★ Andrew Collier Cameron,[1] Stephane Udry,[2] Jean-François Donati,[3] Keith Horne,[1] David James[4] and Alan Penny[5]

[1]*School of Physics & Astronomy, University of St Andrews, North Haugh, St Andrews, Fife, KY16 9SS*
[2]*Observatoire de Genève, 51 ch. des Maillettes, 1290 Sauverny, Switzerland*
[3]*Laboratoire d'Astrophysique Observatoire Midi-Pyrénées, 14 avenue Edouard Belin, F-31400 Toulouse, France*
[4]*Observatoire de Grenoble, F-38041 Grenoble, Cedex 9, France*
[5]*Rutherford Appleton Laboratory, Chilton, Didcot, Oxon OX11 0QX*

Accepted 2003 October 9. Received 2003 October 7; in original form 2003 September 18

**ABSTRACT**

We have used a Doppler tomographic analysis to conduct a deep search for the starlight reflected from the planetary companion to HD 75289. In four nights on VLT(UT2)/UVES in 2003 January, we obtained 684 high-resolution echelle spectra with a total integration time of 26 h. We establish an upper limit on the geometric albedo of the planet $p < 0.12$ (to the 99.9 per cent significance level) at the most probable orbital inclination $i \simeq 60^\circ$, assuming a grey albedo, a Venus-like phase function and a planetary radius $R_p = 1.6\ R_{Jup}$. We are able to rule out some combinations of the predicted planetary radius and atmospheric albedo models with high, reflective cloud decks.

**Key words:** techniques: spectroscopic – stars: individual: HD 75289 – planetary systems.

## 1 INTRODUCTION

The existence of a close planetary companion to the G0 V star HD 75289 was first reported by Udry et al. (2000). In common with 19 of the 117 extrasolar planets known, HD 75289b is found to orbit within 0.1 au of its parent star. Confirmation of the gas giant nature of the close-orbiting exoplanet HD 209458b (Charbonneau et al. 2000; Henry et al. 2000) suggests that similar objects may reflect enough starlight to allow a direct planetary detection. Spectral models of these 'Pegasi planets' (Barman et al. 2002; Sudarsky, Burrows & Hubeny 2003) show that scattered starlight dominates over thermal emission at optical wavelengths. Sudarsky et al. (2003) suggest that the high effective temperature and relatively low surface gravity of HD 75289b may favour the formation of relatively bright, high-altitude silicate cloud decks, which act to scatter starlight back into space before being absorbed by alkali metals in the deeper atmosphere.

Here we report the results of observations, conducted over four nights in 2003 January on the VLT2/UVES echelle spectrograph, aimed at detecting the starlight reflected from HD 75289b. In Section 2 we summarize the basic physics that underpins our analysis, whilst Sections 3 and 4 review the acquisition, reduction and processing of the raw echelle spectra, using techniques described more comprehensively in Collier Cameron et al. (2002) and Leigh et al. (2003a). Finally, in Section 5 we use our results to place upper limits on the grey geometric albedo of the planet.

★E-mail: cjl5@st-andrews.ac.uk

## 2 SYSTEM PARAMETERS

HD 75289 (HIP 43177) is a G0 main-sequence star with parameters listed in Table 1. High-precision radial-velocity (RV) measurements obtained between 1998 November and 1999 October (Udry et al. 2000) were used to identify a planetary companion HD 75289b, the properties of which (as determined directly from RV studies or inferred using the estimated stellar parameters) are also summarized in Table 1. Since the publication of the planet (Udry et al. 2000), the orbital solution has been updated with new Coralie RV measurements using a weighted cross-correlation scheme (Pepe et al. 2002) with an appropriate template.

As the planet orbits its host star, some of the starlight incident upon its surface is reflected towards us, producing a potentially detectable signature within the observed spectra of the star. This signature takes the form of faint copies of the stellar absorption lines, Doppler-shifted because of the orbital motion of the planet and greatly reduced in intensity as a result of the small fraction of starlight that the planet intercepts and reflects back into space.

With our knowledge of the stellar mass and the orbital period of the planet, we can estimate the orbital velocity of the planet $V_p$ (see Collier Cameron et al. 2002). The apparent RV amplitude $K_p$ of the reflected light is given by

$$K_p = V_p \sin i = 147 \sin i \ \mathrm{km\ s^{-1}}, \quad (1)$$

where the orbital inclination $i$ is, according to the usual convention, the angle between the orbital angular momentum vector and our line of sight.

For all but the lowest inclinations, the orbital velocity amplitude of the planet is much greater than the broadened widths of the stellar

**Table 1.** System parameters (and uncertainties) for HD 75289 and its planetary companion.

| | |
|---|---|
| **Star** | |
| Spectral type | G0 V[1] |
| $m_v$ | 6.35 (0.013)[2,3] |
| Distance (pc) | 28.9 (0.46)[2] |
| $T_{\rm eff}$ (K) | 6135 (40)[4] |
| $M_*(M_\odot)$ | 1.22 (0.05)[5,6,7] |
| $R_*(R_\odot)$ | 1.25 (0.05)[5,6,7] |
| [Fe/H] | 0.27 (0.06)[4] |
| $P_{\rm rot}$ (d) | 16.0 (3.0)[8,9] |
| v sin $i$ (km s$^{-1}$) | 3.8 (0.6)[10] |
| Age (Gyr) | 5.6(1.0)[8,11] |
| **Planet** | |
| Orbital period $P_{\rm orb}$ (d) | 3.5091 (0.0001)[10] |
| Transit epoch $T_0$ (JD) | 52651.1566 (0.1251)[10] |
| $K_*$(m s$^{-1}$) | 53.4 (0.6)[10] |
| $a$ (au) | 0.0483 (0.0020)[10] |
| $M_{\rm p}$ sin $i$ ($M_{\rm Jup}$) | 0.455 (0.028)[10] |

References: [1]Gratton, Focardi & Bandiera (1989); [2]ESA (1997); [3]Gray, Napier & Winkler (2001); [4]Santos, Israelian & Mayor (2001); [5]Fuhrmann, Pfeiffer & Bernkopf (1998); [6]Gonzalez & Laws (2000); [7]Gonzalez et al. (2001); [8]Udry et al. (2000); [9]Noyes et al. (1984); [10]Udry et al. (2000), revised for this paper; [11]Donahue (1993).

absorption lines. Hence lines in the reflected-light spectrum of the planet should be Doppler-shifted well clear of their stellar counterparts, allowing a clean spectral separation for most of the orbit.

By isolating the reflected planetary signature, we are in effect observing the planet–star flux ratio ($\epsilon$) as a function of orbital phase ($\phi$) and wavelength ($\lambda$), where

$$\epsilon(\alpha,\lambda) \equiv \frac{f_{\rm p}(\alpha,\lambda)}{f_\star(\lambda)} = p(\lambda)g(\alpha,\lambda)\frac{R_{\rm p}^2}{a^2}. \quad (2)$$

The phase function $g(\alpha,\lambda)$ describes the variation in the planet–star flux ratio with the phase angle $\alpha$; here $\alpha$ is the angle subtended at the planet by the star and the observer, and varies as $\cos\alpha = -\sin i\cos\phi$. As the shape of $g(\alpha,\lambda)$ is unknown, current practice is to adopt a specific phase function in order to express the results in terms of the planet–star flux ratio that would be seen at phase angle zero:

$$\epsilon_0(\lambda) = p(\lambda)\frac{R_{\rm p}^2}{a^2}, \quad (3)$$

where $p(\lambda)$ is the wavelength-dependent geometric albedo and the orbital distance $a$ is constrained by Kepler's third law. For reasons described by Collier Cameron et al. (2002) and Leigh et al. (2003a), the $g(\alpha,\lambda)$ that we adopt is a polynomial approximation to the empirically determined phase function for Venus (Hilton 1992).

In the event of a planetary detection, analysis of the data should allow us to determine two fundamental properties:

(i) $K_{\rm p}$, the projected orbital velocity of the planet, from which we obtain the system inclination and planetary mass, since $M_{\rm p}$ sin $i$ is known from the Doppler wobble of the star;

(ii) $\epsilon_0$, the maximum flux ratio observed where, by making theoretical assumptions about the nature of the planet, we can invoke equation (3) to constrain $R_{\rm p}$ or $p$.

## 3 OBSERVATIONS

We observed HD 75289 during 2003 January using the blue arm of the UV–Visual Echelle Spectrograph (UVES), mounted on the 8.2-m VLT/UT2 (Kueyen) telescope at the Paranal Observatory in Chile. The detector was a single EEV CCD-44 array windowed to an image format of 2048 × 3000 15.0-μm pixels, and centred at 475.8 nm in order 102 of the 41.6 line mm$^{-1}$ echelle grating, giving good wavelength coverage from 406.5 to 522.0 nm. For reasons described in greater detail by Collier Cameron et al. (2002), we believe that the prominence of Rayleigh scattering, combined with the high density of absorption lines within this spectral range, offers the best chance of detection. With an average pixel spacing close to 1.5 km s$^{-1}$, the FWHM intensity in the central orders of the thorium–argon calibration spectra was found to be 4.5 pixels, suggesting an effective resolving power $R = 43\,000$.

**Table 2.** Journal of observations. The UTC mid-times and orbital phases are shown for the first and last spectral exposures secured on each night of observation in 2003 January. The number of exposures is given in the final column.

| UTC start | Phase | UTC end | Phase | $N_{\rm exp}$ |
|---|---|---|---|---|
| Jan 14 01:00:04 | 0.396 | Jan 14 09:29:44 | 0.497 | 188 |
| Jan 15 00:56:42 | 0.680 | Jan 15 09:21:32 | 0.780 | 173 |
| Jan 21 02:40:18 | 0.410 | Jan 21 09:34:54 | 0.492 | 183 |
| Jan 22 03:35:30 | 0.706 | Jan 22 09:41:01 | 0.778 | 140 |

Table 2 details the four nights of observations that contribute to this analysis. Each of the stellar spectra were exposed between 100 and 300 s, depending upon the seeing, in order to expose the CCD to ∼40 000 ADU pixel$^{-1}$ in the brightest parts of the image. A typical exposure in average seeing (0.8 arcsec) yielded ∼4 × $10^5$ electrons per pixel step in wavelength in the brightest orders after extraction. The 7-s fast-readout time of the CCD allowed an observing efficiency > 90 per cent, and saw a gain of 2.4 and readout noise of ∼ 6 e$^-$.

## 4 DATA PROCESSING

One-dimensional spectra were extracted from the raw images using an automated pipeline reduction system built around the Starlink ECHOMOP and FIGARO packages.

After initial tracing of the echelle orders, an extraction process subtracted the bias from each frame, cropped it, determined the form and location of the stellar profile on each image, subtracted a linear fit to the scattered light + sky background across the spatial profile, and performed an optimal (profile and inverse variance-weighted) extraction of orders across the full spatial extent of the object+sky region. In all, 25 orders (numbers 90–114) were extracted from each image, giving good spectral coverage from 406.5 to 522.0 nm. Following extraction, the signal-to-noise ratio in the continuum of the brightest orders was typically 650 per pixel step.

Flat-field balance factors were applied prior to extraction by summing the 50–100 flat-fields taken at the start and end of each night. Although the UVES instrument was very stable between observations, we found that the noise was slightly reduced (∼2 per cent) by the use of nightly flat-fields rather than master flat-fields combining the data from all four nights.

### 4.1 Extracting the planetary signal

The first step in extracting the reflected component is to subtract the direct stellar component from the observed spectrum. The planetary signal should then consist of faint Doppler-shifted copies of each of the stellar absorption lines, at this stage buried deeply in the

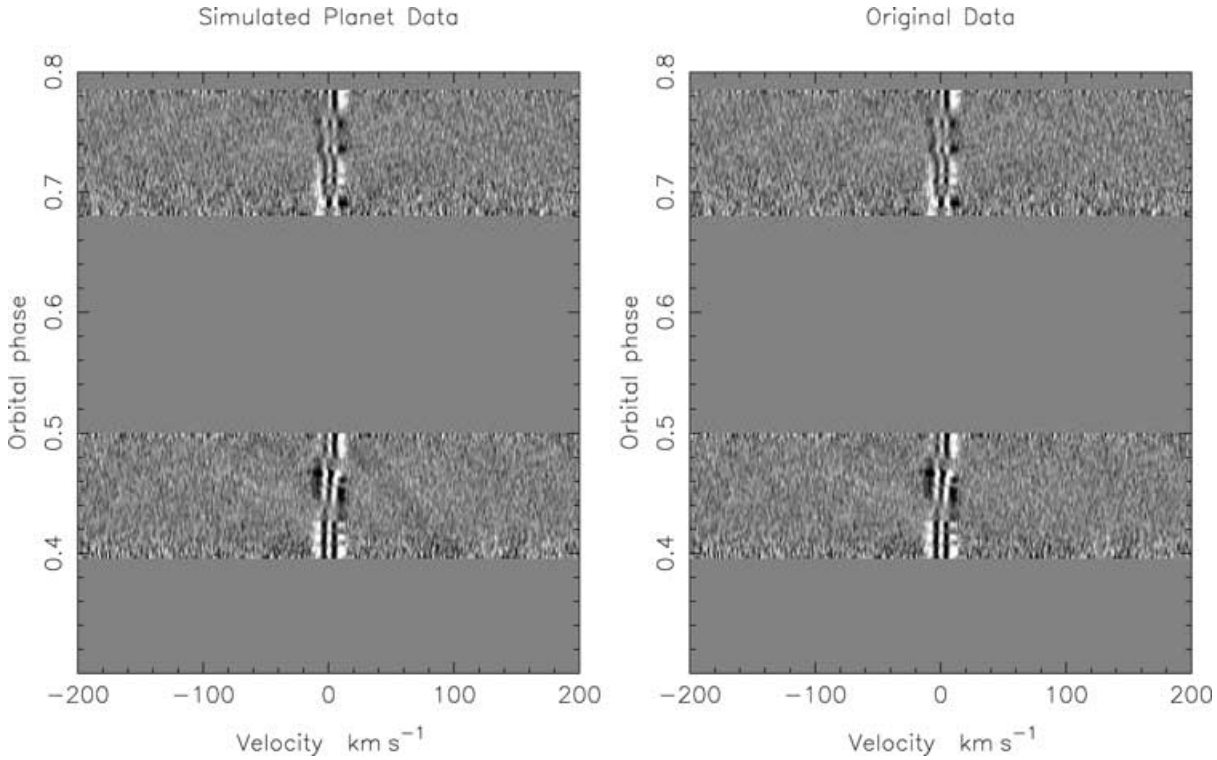


**Figure 1.** Time series of deconvolved profiles derived from the VLT(UT2)/UVES spectra, secured over four nights in 2003 January. The left-hand plot demonstrates the result of adding a simulated planet signal at an inclination of 80°, assuming grey geometric albedo $p = 0.4$ and a radius of 1.6 $R_{Jup}$. The planetary signature appears as a dark sinusoidal feature crossing from right to left as phase increases and centred on the superior conjunction at phase 0.5. The right-hand plot shows the original data, where no such trail is evident. The grey-scale runs from black at $-10^{-4}$ times the mean stellar continuum level, to white at $+10^{-4}$. The velocity scale is in the reference frame of the star.

noise. A detailed description of this procedure is given by Collier Cameron et al. (2002), appendix A. After cleaning any correlated fixed-pattern noise remaining in the difference spectra (see Collier Cameron et al. 2002, appendix B), we create a composite residual line profile by deconvolving each residual spectrum with a list of stellar absorption-line strengths (Collier Cameron et al. 2002, appendix C). The deconvolution results in a 32-fold improvement in the signal-to-noise ratio, by combining the properties of 2360 images of 1744 absorption lines listed within the observed wavelength range. The composite line profiles are then stacked by phase to display temporal variations in brightness and RV, as in Fig. 1. Any planetary signal present appears as a dark sinusoidal feature in velocity space centred on the superior conjunction at phase 0.5.

The central pattern of distortions in Fig. 1 is consistent with subpixel shifts in the position of the stellar spectra with respect to the detector over the course of the night. Fortunately they only affect a range of velocities at which the planetary signature would in any case be indistinguishable from that of the star.

### 4.2 Simulated planetary signatures

We have verified that a planetary signal is preserved through the above sequence of operations, in the presence of realistic noise levels, by adding a simulated planetary signal to the observed spectra (Fig. 1, left-hand panel). The fake signal also acts to calibrate the strength of any genuine observations and the associated confidence contours. Detailed explanations of the simulated planet calibration can be found in Collier Cameron et al. (2002) and Leigh et al. (2003a). To ensure a strong signal we used a simulated planet of radius 1.6 $R_{Jup}$ and wavelength-independent geometric albedo $p = 0.4$, which when viewed at zero phase angle should give a planet–star flux ratio $\epsilon_0 = f_p/f_* = 9.71 \times 10^{-5}$.

Except for the case of a tidally locked system, any relative motion between the surface of the planet and the surface of the star will result in a difference between the linewidths of the incident and reflected spectra. From the known stellar parameters (Table 1), we have conducted Monte Carlo trials to estimate that the reflected component within the HD 75289 spectra will exhibit typical linewidths close to 13 km s$^{-1}$. In order to mimic the reflected starlight correctly, we have selected the more quickly rotating G0 V star HD 1461 as our planetary template – a star that is of very similar temperature and elemental abundance to HD 75289.

### 4.3 Matched-filter analysis

The next step involves a matched-filter analysis, described by Collier Cameron et al. (2002) (appendix D), to search for features in the time series of composite residual profiles whose temporal variations in brightness and RV resemble those of the expected reflected-light signature.

The relative probabilities of the $\chi^2$ fits to the data for different values of the free parameters $R_p/a$ and $K_p$ are conveniently displayed in grey-scale form as a function of $K_p$ and $\log\ \epsilon_0 = \log\ p(R_p/a)^2$. Fig. 2 details the probability map for the simulated (left) and original (right) observations, normalized to the $\Delta\chi^2$ of the best-fitting model.

To set an upper limit on the strength of any planetary signal, or to assess the likelihood that any signal detection is spurious, we need

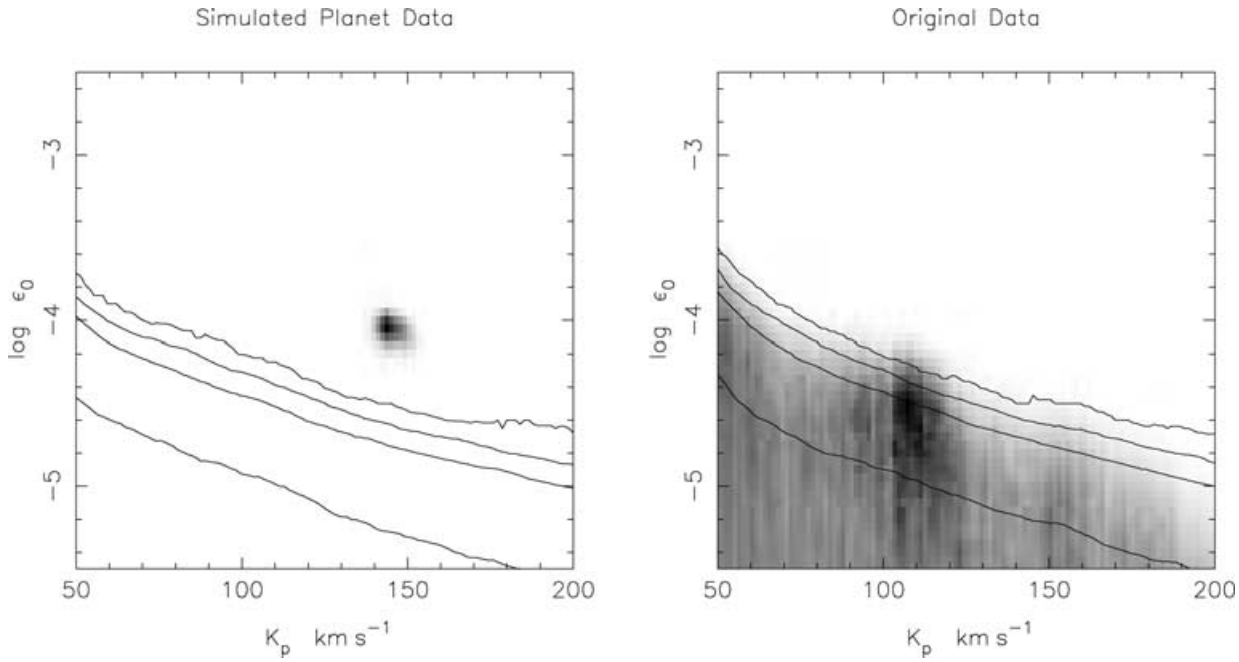


**Figure 2.** Relative probability map of model parameters $K_p$ and $\log \epsilon_0 = \log p(R_p/a)^2$, derived from the VLT(UT2)/UVES observations of HD 75289. The grey-scale denotes the probability relative to the best-fitting model, increasing from 0 for white to 1 for black. The contours show the confidence levels at which spurious detections due to non-Gaussian noise can be ruled out. From top to bottom, they show the 99.9, 99.0, 95.4 and 68.4 per cent confidence limits on $\epsilon_0$ for fixed $K_p$. The left-hand plot demonstrates how the simulated planet signal is recovered through the analysis with ease, and is detected well above the 99.9 per cent confidence limit. The right-hand plot containing the original data, however, demonstrates little evidence for a planetary detection. It is important to note that the contours only give the probability of a false detection if the value of $K_p$ is known in advance, which is not the case here. The slightly increased probability density seen close to $K_p = 110$ km s$^{-1}$ [within the $K_p$ distribution predicted by Leigh et al. (2003b)] returns a large false-alarm probability of 32 per cent when considering all plausible values $35 < K_p < 147$ km s$^{-1}$, which is far too uncertain to claim as genuine.

to compute the probability of obtaining similar improvements in $\chi^2$ by chance alone. We achieve this using a 'bootstrap' procedure to construct empirical distributions for confidence testing, using the data themselves. In 3000 trials, we randomize the order in which the 684 observations were secured, but associated them with the original sequence of dates and times. Genuine signals are scrambled in phase, but re-ordered data are as capable as the original data of producing spurious detections through chance alignments of systematic errors along a sinusoidal path through the data. We record the least-squares estimates of $\log \epsilon_0$ and the associated $\chi^2$ as functions of $K_p$ in each trial.

The percentage points of the resulting bootstrap distribution are shown as contours in Fig. 2. From bottom to top, the contours represent the 68.4, 95.4, 99.0 and 99.9 per cent bootstrap upper limits on the strength of the planetary signal. Thus the 99.9 per cent contour represents the value of $\log \epsilon_0$ that was exceeded in only three of the 3000 trials at each $K_p$.

## 5 RESULTS

The results of this analysis appear in the form of a relative probability map of model parameters $K_p$ and $\log \epsilon_0 = \log p(R_p/a)^2$, shown in Fig. 2. The calibrated confidence contours allow us to apply constraints to the geometric albedo of the planet, given certain theoretical assumptions about the system.

### 5.1 Upper limits on grey albedo

The grey albedo model makes the unlikely assumption that the planet–star flux ratio remains independent of wavelength. By adopting a theoretical radius for the planet, we can use equation (3) to constrain its geometric albedo. Fig. 3 details the upper limits on the albedo at the 99.9 per cent level of significance, for a range of possible inclinations and radii.

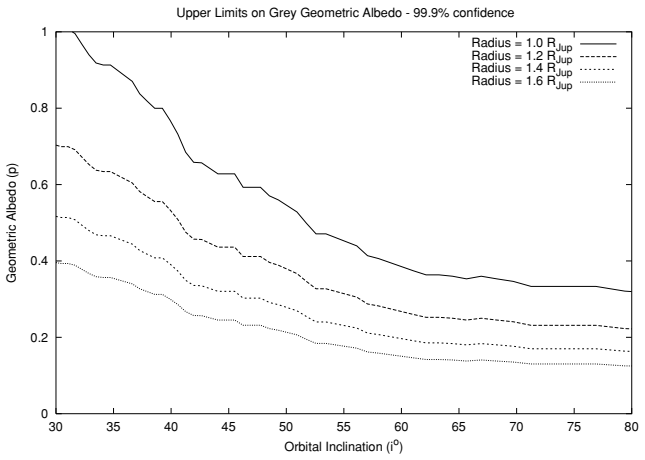


**Figure 3.** Upper limits (99.9 per cent confidence) on the geometric albedo $p$ as a function of inclination and radius, assuming that the atmosphere of the planet imposes no wavelength dependence on reflected light, i.e. a grey albedo model. The contours, from top to bottom, represent upper limits assuming theoretical radii for the orbiting planet of 1.0, 1.2, 1.4 and 1.6 $R_{Jup}$, covering orbital inclinations $30^\circ < i < 80^\circ$. If the planet exhibits the radius, 1.6 $R_{Jup}$, and inclination, $i = 75^\circ$, predicted by Leigh et al. (2003b), then our observations suggest that we can be 99.9 per cent confident of a grey geometric albedo $p < 0.12$.

We find that the albedo limits are less strongly constrained with low-inclination systems. This is a natural consequence of the matched-filter analysis, where fitting such models incorporates more pixels close to the noisier ripples in the central stellar region of the deconvolved profile.

If we adopt the Leigh, Collier Cameron & Guillot (2003b) theoretical radius for HD 75289b of $R_p = 1.6\ R_{Jup}$, we find that the planet–star flux ratio, at the most probable $K_p \simeq 127$ km s$^{-1}$, is constrained to $f_p/f_* < 4.18 \times 10^{-5}$ at the 99.9 per cent level, i.e. a geometric albedo less than 0.12. This would strongly rule out atmospheric models that incorporate high-altitude, reflective cloud decks such as the Class V model of Sudarsky, Burrows & Pinto (2000).

## 6 CONCLUSION

We have observed HD 75289 over four nights in 2003 January, using the VLT(UT2)/UVES instrument, in an attempt to detect starlight reflected by the known close-orbiting planetary companion. The excellent stability of the spectrograph, combined with the reasonable observing conditions, has enabled us to produce deep upper limits on the geometric albedo of the planet. In truth, with our knowledge of the system and current theoretical predictions, we would have expected a reasonably unambiguous detection of the planet. However, we find very little evidence to suggest its presence. Possible reasons for the discrepancy are as follows.

(i) The inclination of the system may be such that the spectral features of the planet do not cleanly separate from the stellar features, i.e. maximum Doppler shift is not sufficient to disentangle the planetary signal. However, evidence generated (Leigh et al. 2003b) using the known system parameters suggests an inclination $i \gg 20^\circ$.

(ii) Our choice of phase function $g(\alpha, \lambda)$ may be wrong. It may be that close-orbiting Pegasi planets are less prone to back-scatter incoming starlight than we see with Jupiter or Venus (Hovenier 1989; Seager, Whitney & Sasselov 2000).

(iii) Although the transiting planet HD 209458 has indicated the presence of a gas giant, it may be that HD 75289b is a more compact terrestrial planet reflecting substantially less starlight (see Guillot et al. 1996).

(iv) It could be that the geometric albedo is inherently low [cf. Class IV model of Sudarsky et al. (2000)], with starlight absorbed deep in the atmosphere of a planet where no high-level clouds are present to reflect the incident light. However, at the wavelengths observed, we do expect a more significant contribution from Rayleigh scattering.

Whatever the cause of the discrepancy, these observations provide a strong test for developing theoretical models which aim to predict the atmospheric nature of these objects. This is a field in desperate need of continued observations on the brightest of these Pegasi planets, as are detailed in the work of Leigh et al. (2003b).

## ACKNOWLEDGMENTS

This work is based on observations with the VLT/UT2 (Kueyen) telescope, provided by the European South Observatory at the Paranal Observatory on Cerro Paranal in the Atacama Desert, Chile. All data processing was conducted using Starlink Project supported hardware and software. ACC and KH were supported by PPARC Senior Fellowships and CL by a PPARC Postgraduate Studentship during the course of this work.

## REFERENCES

Barman T., Hauschildt P., Schweitzer A., Stancil P., Baron E., Allard F., 2002, ApJ, 569, 51
Charbonneau D., Brown T., Latham D., Mayor M., 2000, ApJ, 529, 45
Collier Cameron A., Horne K., Penny A., Leigh C., 2002, MNRAS, 330, 187
Donahue R., 1993, PhD thesis, New Mexico State University
ESA, 1997, The *Hippacos* Catalogue, ESA SP-1200. ESA, Noordwijk
Fuhrmann K., Pfeiffer J., Bernkopf J., 1998, A&A, 336, 942
Gonzalez G., Laws C., 2000, AJ, 119, 390
Gonzalez G., Laws C., Tyagi S., Reddy B., 2001, AJ, 121, 432
Gratton R., Focardi P., Bandiera R., 1989, MNRAS, 237, 1085
Gray R., Napier M., Winkler L., 2001, AJ, 121, 2148
Guillot T., Burrows A., Hubbard W., Lunine J., Saumon D., 1996, ApJ, 459, 35
Henry G., Marcy G., Butler P., Vogt S., 2000, ApJ, 529, 41
Hilton J., 1992, Expanatory supplement to Astronomical Almanac. University Science Books, Mill Valley, CA
Hovenier J., 1989, A&A, 214, 391
Leigh C., Collier Cameron A., Horne K., Penny A., James D., 2003a, MNRAS, 344, 1271
Leigh C., Collier Cameron A., Guillot T., 2003b, MNRAS, 346, 890
Noyes R., Hartmann L., Baliunas S., Duncan D., Vaughan A., 1984, ApJ, 279, 763
Pepe F., Mayor M., Galland F., Naef D., Queloz D., Santos N., Udry S., 2002, A&A, 388, 632
Santos N., Israelian G., Mayor M., 2001, A&A, 373, 1019
Seager S., Whitney A., Sasselov D., 2000, ApJ, 540, 504
Sudarsky D., Burrows A., Pinto P., 2000, ApJ, 538, 885
Sudarsky D., Burrows A., Hubeny I., 2003, ApJ, 588, 1121
Udry S., Mayor M., Naef D., Pepe F., Queloz D., Santos N., 2000, A&A, 356, 590

This paper has been typeset from a TEX/LATEX file prepared by the author.